Mon. Not. R. Astron. Soc. **311**, 120–134 (2000)

V, R, I and Hα photometry of circumnuclear star-forming regions in four galaxies with different levels of nuclear activity

Angeles I. Díaz,[1] Mar Álvarez Álvarez,[1] Elena Terlevich,[2] Roberto Terlevich,[3]★ Miguel Sánchez Portal[1,4] and Itziar Aretxaga[2]

[1]*Departamento de Física Teórica, C-XI, Universidad Autónoma de Madrid, Cantoblanco, 28049 Madrid, Spain*
[2]*INAOE, Tonantzintla, Ap. Postal 51 y 216, Puebla, Mexico*
[3]*Institute of Astronomy, Madingley Road, Cambridge CB3 0HA*
[4]*LAEFF/INTA, PO Box 50727, 28080 Madrid, Spain*

Accepted 1999 August 5. Received 1999 July 23; in original form 1999 April 28

ABSTRACT

We present photometry, in the *V*, *R* and *I* continuum bands and in the Hα + [N II] emission lines, for a sample of circumnuclear star-forming regions (CNSFR), located in four galaxies with different kinds of activity in their nuclei: NGC 7469 (Seyfert 1), NGC 1068 (Seyfert 2), NGC 7177 (LINER) and NGC 3310 (starburst).

Hα luminosities for the CNSFR range from 0.02 to 7×10^{40} erg s^{-1} (uncorrected for internal extinction), comparable to those observed in other galaxies, with NGC 7177 showing the lowest luminosity in average. No systematic differences in the broad-band colours are found for the CNSFR in the different galaxies, except for those in NGC 3310 which are considerably bluer. This is found to be partially because of a younger stellar population.

The colours have been analysed in the light of theoretical evolutionary synthesis models. In some cases they can be reproduced by single populations with ages ranging between 7 and 300 Myr and modest values of extinction (0.5–1.5 mag). However, in many cases, this population is unable to provide the observed equivalent widths of Hα, which require the presence of a younger population.

In the cases of NGC 1068, 7177 and 7469, acceptable fits are found for a two-burst population model at solar metallicity: the younger burst, with an age between 2 and 8 Myr, provides the bulk of the ionization and the older one (8–20 Myr) is responsible for the continuum light at wavelengths longer than Hβ. The age difference between both populations is around 5–7 Myr and the younger burst involves from 3 to 61 per cent of the total mass of the cluster. This would be consistent with the younger burst being originated by the supernova activity from the previous one. Models of this kind also reproduce the regions in NGC 3310, but for younger ionizing population ages (between 1 and 3 Myr) and a metallicity 0.25 times solar.

In most cases an excess in the observed ($R - I$) colour over the model predicted one is found, which is not consistent with a normal reddening law. If this excess is attributed to the red supergiants present in the older population, this seems to imply that this population is not properly taken into account by the models.

In this two-population scenario there seems to be a trend for the circumnuclear star-forming regions of NGC 3310 (starburst), NGC 1068 (Seyfert 2) and NGC 7469 and NGC 7177 (Seyfert 1 and LINER respectively) to be progressively older. Whether this implies a relation between the evolutionary state of the regions and the nuclear type of the parent galaxy remains to be explored.

Key words: H II regions – galaxies: active – galaxies: nuclei – galaxies: Seyfert – galaxies: starburst.

★ Visiting Professor, INAOE, Puebla, Mexico.

1 INTRODUCTION

Early in 1967, Sérsic & Pastoriza realized that the inner parts of some spiral galaxies showed higher star formation rate than usual, and that this star formation was frequently arranged in a ring or pseudo-ring pattern. This fact seems to correlate with the presence of bars in early-type spiral galaxies (Combes & Gerin 1985; Athanassoula 1992). Computational models that simulate the behaviour of gas in galactic potentials show that nuclear rings may appear as a consequence of matter infall, owing to resonances present at the bar edges. In these places the gas loses angular momentum and falls inwards. If, in addition, two inner Lindbald resonances exist – which usually happens in early spirals – gas will condense between both instead of falling directly into the nucleus; this higher gas density may lead to a higher star formation rate, through interacting molecular clouds (Combes & Gerin 1985) or gravitational fragmentation of the ring (Elmegreen 1994). If no inner Lindbald resonance is present, or a very massive central object dominates the dynamics, gas is allowed to continue falling further into the potential well, and eventually may give rise to a nuclear, instead of circumnuclear, starburst or feed an active galactic nucleus (Telesco, Dressel & Wolstencroft 1993; Elmegreen 1997). In this scenario, the most puzzling problem is explaining the presence of nuclear and circumnuclear activity at the same time since, in order to give rise to a circumnuclear ring, the gas needs to stop their infalling in an inner Lindbald resonance and, to generate a nuclear burst or active nucleus, it must continue getting inwards.

However, nuclear activity and the presence of circumnuclear structures undergoing star formation, are simultaneous phenomena in a large number of galaxies (Arsenault 1989) and their mutual influence and the role played by each of them in the dynamics, and/or the energy balance of the galaxy, are still open questions. Three possibilities have been put forward: (1) The nuclear activity has its origin in the supernova remnants product of the intense star formation rate experienced by the circumnuclear regions of the galaxy (Weedman 1983; Norman & Scoville 1987). (2) The star formation in the circumnuclear regions has been induced by gas and radiation ejected by the active nucleus. (3) Both phenomena are not related to each other.

A possible way to elucidate this matter may be through the study of the general properties and evolutionary state of CNSFR in galaxies with different levels of nuclear activity. Specifically, their age and metallicity can provide important clues about the sequence of appearance of both phenomena: nuclear and circumnuclear activity.

A few studies have been made comparing circumnuclear/'hot spot' and disc H II region populations (e.g. Kennicutt et al. 1989; Mayya 1994) and several studies of circumnuclear rings have been made, using observations obtained from the ground and the *Hubble Space Telescope* (*HST*), to try to characterize the stellar content of every single burst (Barth et al. 1995; Buta & Crocker 1993; Holtzman et al. 1992; González-Delgado & Pérez 1996; García-Vargas et al. 1997); however, not a systematic comparison between the CNSFRs of different emission-line type galaxies has so far been made.

For this study we have selected four nearby galaxies with confirmed circumnuclear star-forming rings and different nuclear type: Seyfert 1 (NGC 7469), Seyfert 2 (NGC 1068), LINER (NGC 7177) and starburst (NGC 3310) to perform a comparative study.

NGC 7469 is a well-studied Seyfert 1 galaxy. Maps of [O III] and Hα show a ring outlined by star-forming regions, with a radius of about 1–2 kpc that surrounds the nucleus (Mauder et al. 1994).This ring seems to be related to a bar observed in the *K* band (2.1 μm) (Wilson et al. 1986). Very Large Array (VLA) observations show this ring to split into individual radio emitting knots (Wilson 1991).

NGC 1068 is one of the best-studied Seyfert galaxies. In 1985 Antonucci & Miller detected broad permitted lines in its polarized spectrum, and since then it has become the representative example of the unified model for active galactic nuclei (AGN). Interestingly enough, a strong Ca II triplet in absorption has also been observed and attributed to the presence of red supergiant stars (Terlevich, Díaz & Terlevich 1990a). It shows, as well, one of the most prominent circumnuclear rings, with a radius of about 1 kpc together with an infrared (IR) bar (Scoville et al. 1988; Planesas, Scoville & Myers 1991). The fact that all these features occur simultaneously in this object makes of it an excellent laboratory for the study of possible interrelations between them.

No many bibliographical notes can be found on NGC 7177, but for seven nuclear star-forming regions observed by Hodge (1982). It also appears in some compilations (Verter 1985; Pogge 1989).

Finally, NGC 3310 is a good example of an overall low-metallicity galaxy, with a high rate of star formation and very blue colours. It is also a prominent source of X Rays and Ultraviolet radiation. The circumnuclear region was studied spectrophotometrically by Pastoriza et al. (1993). The brightest H II region was reported by Terlevich et al. (1990b) to show the IR Ca II triplet in absorption. No presence of nuclear bars has been reported till now and therefore the merging with a low-metallicity object about 18 Myr ago, is proposed as the fuelling mechanism for the nuclear burst (Smith et al. 1996).

In this paper we present photometric results through broad-band *V*, *R*, *I* and narrow Hα filters on a total of 68 regions, distributed on the four galaxy rings. Observations and reduction details are described in Section 2. The results are presented in Section 3 and discussed in Section 4. Finally, the summary and main conclusions of the work are presented in Section 5.

2 OBSERVATIONS AND REDUCTIONS

The observations were made as part of two observing runs in 1988 and 1990 using a blue sensitive GEC CCD at the f/15 Cassegrain focus of the 1.0-m Jacobus Kaptein Telescope (JKT) of the Isaac Newton Group at the Observatorio del Roque de los Muchachos, La Palma. The CCD had 578×385 pixels 22-μm wide. The scale obtained with this instrumental configuration is 0.3 arcsec pixel^{-1}, and the CCD field is 2.89×1.92 arcmin^2. The main characteristics of the sample galaxies are summarized in Table 1. Column 1 gives the galaxy identification; column 2 the morphological type as listed in the Third Reference Catalog of Bright Galaxies (RC3; de Vaucouleurs et al. 1991); column 3 the linear size in parsecs per arcsecond; column 4 the nuclear type; column 5 the total B magnitude (RC3) and column 6, the distance taken from the references given in the table. Finally, column 7 gives the adopted galactic extinction towards the galaxy (see this section below).

Observations and reductions are described in detail in Sánchez Portal et al. (1999) and are outlined in what follows.

All observations were made under photometric conditions, and the seeing was estimated using stars present in each frame. Each night photometric (Landolt 1983) and spectrophotometric (Massey et al. 1988; Stone 1977) standards were observed to perform the corresponding calibrations. We also took dome and sky flat-field

Table 1. Characteristics of the sample.

Galaxy	Morphological type	pc arcsec^{-1}	Nuclear Type	B_T	D (Mpc)	$E(B-V)_{\rm gal}$
NGC 1068	(R)SA(rs)b	87.8	Sy2	9.61	18.1[1]	0.05
NGC 3310	SAB(r)bc pec	60.6	Starburst	11.15	12.5[2]	0.00
NGC 7177	SAB(r)b	74.2	LINER	12.01	15.3[3]	0.23
NGC 7469	(R')SAB(rs)a	315.12	Sy1	13.00	65.0[4]	0.12

Notes to Table 1:
1 – Sandage & Tammann (1975).
2 – Bottinelli et al. (1984).
3,4 – NED[a] $H_0 = 75\,{\rm km\,s^{-1}}$ Mpc.
[a] The National Extragalactic Database (NED), is operated by the Jet Propulsion Laboratory, California Institute of Technology, under contract with the National Aeronautics and Space Administration.

Table 2. Journal of observations.

Galaxy	Filter	exposure time (s)	seeing ($''$)
NGC 1068	*V*	100	2.1
	R	100	2.1
	I	100	2.1
	LINE	800	1.2
	CONT	800	1.2
NGC 3310	*V*	200	1.02
	R	300	1.02
	I	300	1.02
	LINE	700	1.02
NGC 7177	*V*	600	1.2
	R	600	1.2
	I	600	1.0
	LINE	2000	1.3
	CONT	2000	1.4
NGC 7469	*V*	500	1.3
	R	300	1.3
	I	300	1.3
	LINE	800	1.5
	CONT	1000	1.5

images as well as zero exposure time frames to set the bias level.

Images in the broad *V*, *R* and *I* and narrow Hα and continuum filters were obtained for every galaxy, except in the case of NGC 3310, for which no Hα continuum image was taken. A journal of observations is presented in Table 2. The filter characeristics are given in Table 3. Columns 1 to 4 give, respectively, the filter name, central wavelength and full width at half maximum (FWHM) in angstroms, and maximum transmission. The Hα filter includes the lines of [N II] at $\lambda\lambda$ 6548, 6584 Å although the latter enters the filter at about half transmission. The typical value of the [N II] λ 6548 Å line in H II regions is at most 1/2 of Hα.

The data reduction was carried out using IRAF and MIDAS routines following the standard steps: subtraction of the bias level, flat-field division and sky background removal that was performed by averaging the mean count values in several boxes in the outer parts of each frame. Later on, cosmic rays were removed, the point spread function (PSF) was estimated using stellar images in each frame, and flux calibration was performed.

Both atmospheric and galactic extinction corrections were applied. The first one using the extinction coefficients provided by La Palma Observatory, and the second one using the values of $E(B-V)$ taken from Burstein & Heiles (1984; see Table 1) and the galactic extinction curve of Seaton (1979). No internal absorption correction was attempted.

Table 3. Filter characteristics.

Filter	$\lambda_{\rm c}$(Å)	FWHM (Å)	$\tau_{\rm max}$ (%)
V	5470	938	80
R	6455	1253	87
I	8300	1813	85
Hα ($v_{\rm r} = 0\,{\rm km\,s^{-1}}$)	6563	53	50
Hα ($v_{\rm r} = 4000\,{\rm km\,s^{-1}}$)	6652	49	54

3 RESULTS

3.1 H II region photometry

Hα frames were continuum subtracted in order to obtain a net Hα line image. Hα continuum images were available for NGC 1068, 7177 and 7469. In the case of NGC 3310, a continuum frame was constructed from the broad-band *R* image as explained in Terlevich et al. (1991). In all cases the two images to be subtracted were previously aligned according to the offsets derived from the centroids of a bidimensional gaussian fit to the field star images.

Fig. 1 shows the Hα line contour maps for the four observed galaxies. Individual H II regions are marked and labelled. In the images, north is to the top and east is to the left.

In the four studied galaxies the CNSFRs are arranged in a ring pattern. The biggest ring, with a mean radius of 2 kpc, is found in NGC 7469, followed by that of NGC 1068, with a mean radius of 1.8 kpc. Smaller rings are found for NGC 7177 and 3310, with mean values of about 0.8 kpc. The rings of NGC 7469, 1068 and 3310 are almost circular, while that of NGC 7177 shows a more distorted morphology.

Star-forming regions have been identified on Hα line images and their fluxes have been measured. When computing the sizes and fluxes of these regions, three main problems were encountered.

(i) Photometry software packages are not very efficient to measure fluxes from diffuse objects in a non-constant background.
(ii) In very crowded regions, deciding the limits of two adjacent regions is almost arbitrary.
(iii) Even in isolated regions, the determination of their radii is always difficult.

Theoretically, a radiation bound H II region, can be characterized by its Strömgren radius. But, in practice, they show a bright core, surrounded by a more extended and dimmer region. The border radius between them can only be distinguished in isolated

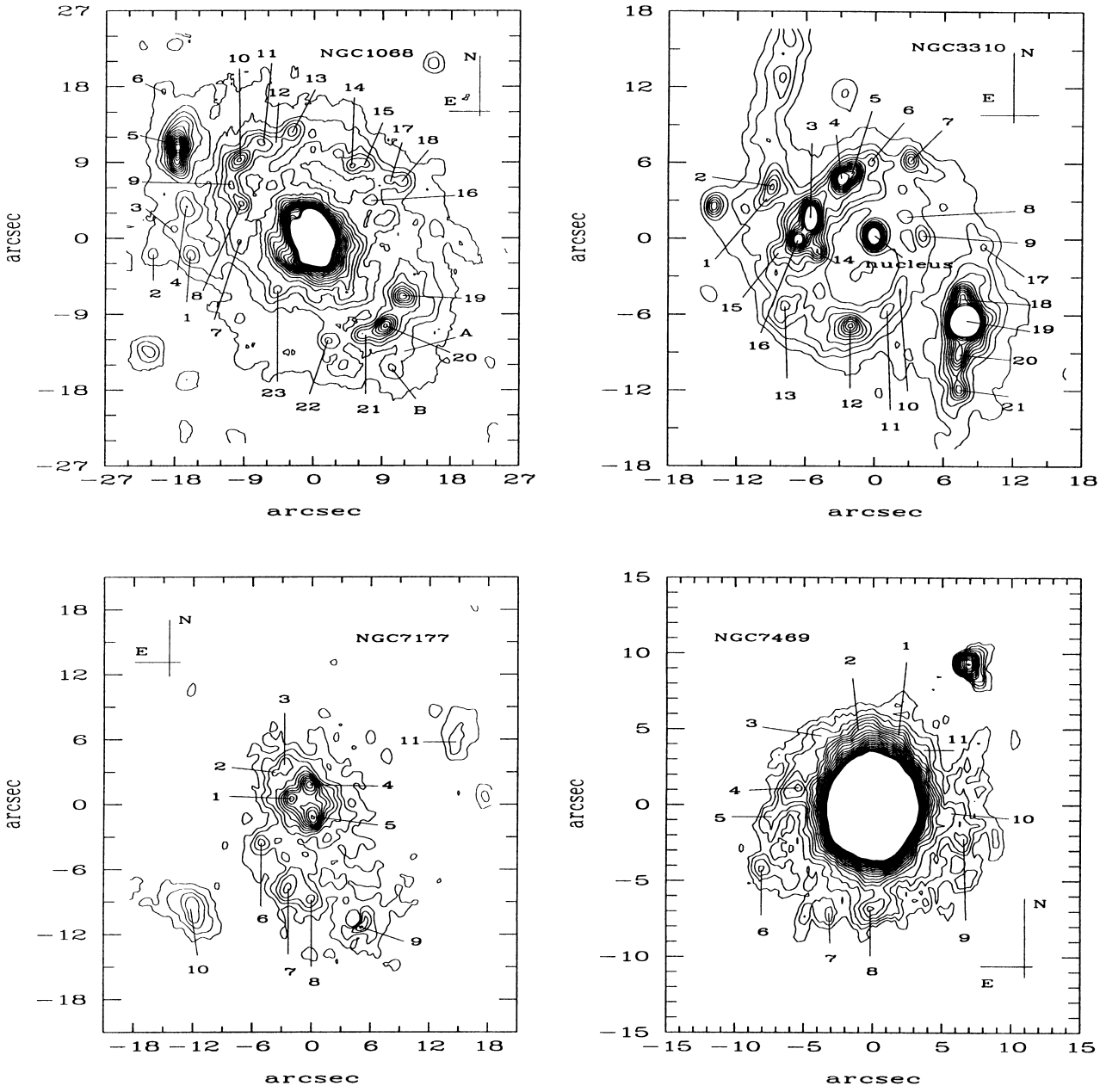

Figure 1. Isophotal maps of (a) NGC 1068, (b) NGC 3310, (c) NGC 7177 and (d) NGC 7469 with H II region identification labels.

and not distorted regions. This can be seen in Fig. 2 where we have plotted flux (in arbitrary units) versus radius for H II regions of different morphologies.

Taking this into account, we have followed different criteria in order to determine the H II region sizes and fluxes. In isolated regions, we have computed the Hα flux inside circular apertures of different radii.[1]

In the plot of flux versus radius (Fig. 2), an asymptotic behaviour can be seen. For most observed regions the asymptotic radius is reached when the flux falls down to 10 per cent of the flux at the central pixel. We have taken this radius as the radius of the region, and the flux inside it as the region flux.

When the morphology of the region is distorted (see NGC 7469 #2 in Fig. 2), we have added all the flux inside a circular aperture up to the isophote corresponding to 10 per cent of the central value, even though the minimum could be lower. When two regions are very close to each other we have computed their flux together if the minimum signal along the line that joins the two central pixels is higher than 50 per cent of the smaller maximum. In all other cases, we have integrated both regions separately.

Once the sizes and Hα fluxes of every region were measured, Hα equivalent widths – computed by division of the Hα line frame by the corresponding continuum image – were also obtained. As already mentioned above, no Hα continuum image was available for NGC 3310. In this case the Hα equivalent width was calculated using the *R* filter as described in Bessell (1990).

[1] Owing to software limitations no circular regions could be integrated interactively, so we used square boxes instead. Radius stands for the equivalent radius of the circular region having the same area as the square one. $r = \sqrt{\text{area}/\pi}$.

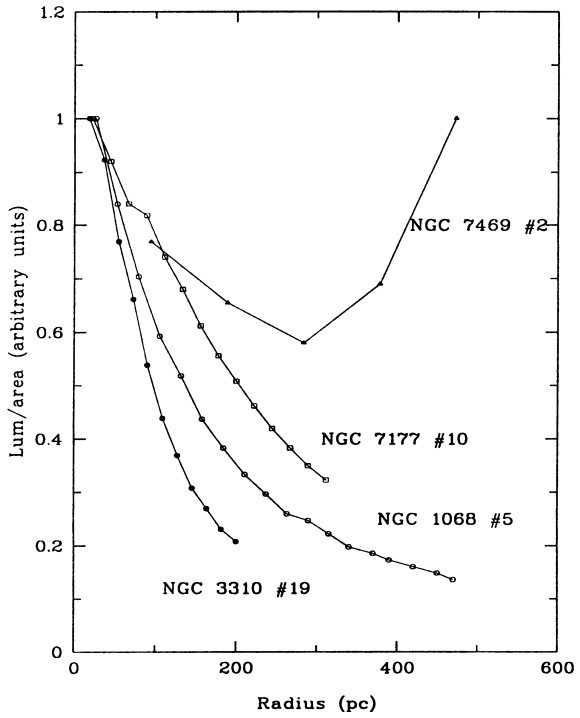

Figure 2. Radial brightness profiles for selected H II regions. Hα luminosity per unit area versus radius is plotted. The most regular behaviour corresponds to the biggest and most isolated regions of NGC 3310, 1068 and 7177. The asymptotic radius is reached when the flux is about 10 per cent of the flux in the central pixels of each region. The rise in the NGC 7469 region # 2 profile is owing to the contribution of the nuclear flux.

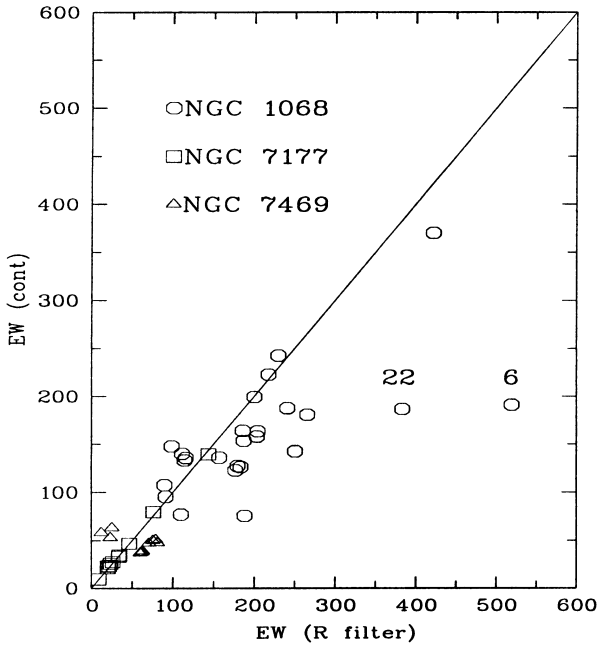

Figure 3. Equivalent width of the line obtained using the continuum frame, versus that obtained using the *R* filter for NGC1068, 7177 and 7469. The solid line stands for EW(cont) = EW(*R* filter). The scattering in the points is possibly becasue of insufficient background computation or slight missalignment.

The two methods yield slightly different results. This can be seen in Fig. 3 where we plot the equivalent width of Hα derived using its corresponding continuum, EW(cont), against that calculated using the *R*-band image as continuum, EW(*R*). The solid line stands for EW(cont) = EW(*R*), while the best linear regression fit gives EW(cont) = 0.77 EW(*R*) + 12.3 Å. Outlying regions 6 and 22 in NGC 1068 present an anomalous behaviour. Both are faint and are located in the direction of the ionization cone subtended by the nuclear radiation. They have not been taken into account in computing the fit and have been excluded from the general study.

In order to measure the broad-band fluxes, all the frames were carefully aligned as explained above, and the corresponding fluxes were measured inside the apertures defined on the Hα line frame. Subsequently, the broad-band magnitudes were computed and these magnitudes were subtracted to obtain the colours.

Sizes and distances from the galactic nucleus[2] (in arcsec), *V* magnitudes, broad-band colours, Hα fluxes (in erg s^{-1} cm^{-2}), and Hα equivalent widths (in Å) computed in the described way are listed in Table 4 for every detected H II region in each observed galaxy.

We have estimated the background contribution to the computed magnitudes from the observed intensity radial profiles (Sánchez Portal et al. 1999) for each galaxy. The average contribution is about 10 per cent and the maximum contribution has been found for region # 2 in NGC 7177 amounting to about 40 per cent in the *I* band. This region is faint and located close to the bulge of the galaxy. The mean background colours for NGC 7177 are $V - V = 0.4$ and $R - I = 0.65$ (Sánchez Portal et al. 1999), therefore the background subtracted colours of the region are about 0.03 mag redder than computed without taking this contribution explicitly into account.

In fact, the main source of error in this work comes from the determination of the radius for each H II region. Therefore, in order to estimate realistic errors, the fluxes inside the adopted radius plus and minus one pixel have also been computed for each region. We have adopted as errors the differences between the two calculated extreme values. These errors are also listed in Table 4. This procedure effectively takes into account the contribution by any local variable background.

R frames were further corrected for the contribution of Hα + [N II] emission using the Hα line image as explained in Terlevich et al. (1991). In most cases this correction amounts to only 0.1 mag.

3.2 Characteristics of the CNSFRs

Angular sizes and galactocentric radii, apparent magnitudes and Hα fluxes have been converted to linear quantities, absolute magnitudes and Hα luminosities using the distance to each galaxy given in Table 1, and are listed in Table 5. The quoted linear size corresponds to the aperture radius used for the photometry.

Linear diameters range from 82.4 to 684.8 pc. The size of the largest region in each galaxy decreases from 684.8 pc in NGC 1068 to 182 pc in NGC 3310, with NGC 7469 and 7177 showing intermediate values (428.6 and 252.2 pc respectively).

Hα luminosities range from 2×10^{38} to 7×10^{40} erg s^{-1}. These values are similar to those found for other CNSFRs in galaxies (e.g. González-Delgado et al. 1995). Most of them have

[2] The galactic nucleus has been defined as the maximum of the Hα flux distribution.

Table 4. Observed sizes, magnitudes and Hα fluxes of measured H II regions.

region number	radius (″)	distance from centre (″)	V	$V-R$ (mag)	$R-I$	F(Hα) (erg s^{-1} cm^{-2})	EW(Hα) (Å)
			NGC 1068				
1	1.7	(−17.4,−2.8)	16.5 ± 0.4	0.47 ± 0.02	0.65 ± 0.001	2.2e-13	242.5
2	1.7	(−23.1,−2.4)	17.2 ± 0.5	0.37 ± 0.02	0.58 ± 0.002	1.1e-13	180.6
3	1.7	(−20.4, 0.6)	16.6 ± 0.4	0.40 ± 0.001	0.72 ± 0.01	1.7e-13	222.7
4	1.4	(−18.3, 3.9)	16.4 ± 0.4	0.49 ± 0.02	0.64 ± 0.004	2.1e-13	199.4
5	3.9	(−19.5,11.1)	15.0 ± 0.2	0.41 ± 0.001	0.46 ± 0.02	1.6e-12	369.9
6	–	–	–	–	–	–	–
7	1.5	(−10.8,−0.9)	15.2 ± 0.4	0.37 ± 0.008	0.59 ± 0.01	2.6e-13	95.6
8	1.5	(−10.2, 4.2)	15.6 ± 0.5	0.44 ± 0.008	0.58 ± 0.002	3.2e-13	135.9
9	1.5	(−11.7, 6.9)	15.2 ± 0.5	0.38 ± 0.03	0.60 ± 0.002	3.1e-13	133.0
10	2.2	(−10.8,9.9)	15.0 ± 0.4	0.38 ± 0.008	0.62 ± 0.003	6.1e-13	75.8
11	1.6	(−7.5,12.3)	15.8 ± 0.5	0.46 ± 0.01	0.61 ± 0.02	3.3e-13	153.4
12	0.9	(−5.4,12.6)	16.4 ± 0.6	0.48 ± 0.01	0.64 ± 0.002	1.0e-13	147.6
13	2.0	(−3, 13.8)	16.0 ± 0.5	0.46 ± 0.0006	0.62 ± 0.01	3.5e-13	142.5
14	1.3	(5.4,9.3)	15.3 ± 0.4	0.27 ± 0.02	0.52 ± 0.001	2.1e-13	107.3
15	1.3	(7.8,9.6)	15.6 ± 0.5	0.36 ± 0.002	0.49 ± 0.01	2.2e-13	139.9
16	1.3	(8.7,5.1)	15.7 ± 0.6	0.29 ± 0.01	0.52 ± 0.007	1.7e-13	77.2
17	1.3	(11.1,7.5)	16.4 ± 0.6	0.35 ± 0.02	0.52 ± 0.009	1.6e-13	127.2
18	1.3	(13.2,7.5)	16.8 ± 0.6	0.45 ± 0.002	0.46 ± 0.008	1.6e-13	187.5
19	2.4	(13.5,−7.8)	15.1 ± 0.4	0.56 ± 0.01	0.53 ± 0.008	6.9e-13	163.9
20	2.0	(10.5,−11.7)	14.7 ± 0.3	0.44 ± 0.01	0.54 ± 0.003	5.3e-13	135.6
21	1.6	(7.2,−12.9)	16.2 ± 0.5	0.56 ± 0.0004	0.53 ± 0.02	2.5e-13	157.9
22	–	–	–	–	–	–	–
23	1.3	(−5.1,−7.2)	16.3 ± 0.6	0.45 ± 0.002	0.62 ± 0.0006	1.9e-13	126.2
A	1.3	(13.5,−15.3)	17.0 ± 0.7	0.45 ± 0.002	0.49 ± 0.008	9.9e-14	122.5
B	1.6	(12.0,17.4)	16.6 ± 0.5	0.45 ± 0.02	0.50 ± 0.003	1.6e-13	163.4
			NGC 3310				
1	0.7	(−10.5,2.7)	19.3 ± 0.9	0.32 ± 0.002	0.12 ± 0.03	6.8e-14	953.4
2	1.0	(−9.6,4.2)	17.6 ± 0.5	0.37 ± 0.005	0.13 ± 0.008	1.5e-13	448.7
3	1.4	(−6.0,1.5)	16.3 ± 0.4	0.26 ± 0.03	0.15 ± 0.03	5.4e-13	527.2
4	1.0	(−3.0,4.8)	16.5 ± 0.5	0.21 ± 0.04	0.21 ± 0.01	3.3e-13	426.5
5	0.7	(−2.1,5.4)	17.2 ± 0.9	0.23 ± 0.009	0.23 ± 0.04	1.8e-13	416.4
6	1.0	(−0.3,6.3)	16.9 ± 0.6	0.26 ± 0.01	0.21 ± 0.002	1.3e-13	229.3
7	1.0	(3.3,6.3)	16.9 ± 0.6	0.25 ± 0.004	0.20 ± 0.02	1.2e-13	229.8
8	0.7	(3.0,1.5)	17.5 ± 0.9	0.33 ± 0.005	0.29 ± 0.004	5.2e-14	167.9
9	1.0	(4.5,0.0)	16.9 ± 0.6	0.27 ± 0.03	0.24 ± 0.01	9.3e-14	178.3
10	1.0	(2.4,−4.5)	16.9 ± 0.7	0.34 ± 0.01	0.25 ± 0.007	9.3e-14	164.8
11	1.0	(1.2,−6.6)	16.8 ± 0.6	0.32 ± 0.0004	0.24 ± 0.0009	1.1e-13	180.0
12	1.4	(−2.4,−8.1)	16.0 ± 0.4	0.30 ± 0.6	0.14 ± 0.6	2.9e-13	232.4
13	1.0	(−8.4,−6.0)	16.6 ± 0.6	0.25 ± 0.009	0.15 ± 0.005	1.3e-13	191.8
14	1.0	(−5.4,−1.5)	16.8 ± 0.6	0.36 ± 0.01	0.21 ± 0.009	1.8e-13	257.5
15	0.7	(−9.3,−1.5)	18.5 ± 0.9	0.45 ± 0.01	0.16 ± 0.02	7.7e-14	489.6
16	1.0	(−7.2,−0.3)	17.1 ± 0.6	0.35 ± 0.0006	0.13 ± 0.02	3.3e-13	564.8
17	0.7	(10.2,−0.9)	18.4 ± 0.9	0.29 ± 0.01	0.18 ± 0.03	4.4e-14	328.8
18	1.0	(8.4,−5.1)	16.9 ± 0.6	0.25 ± 0.008	0.09 ± 0.02	2.8e-13	469.5
19	1.7	(8.4,−7.5)	15.7 ± 0.2	0.20 ± 0.02	0.00 ± 0.02	1.2e-12	626.8
20	1.0	(−22.2,-)	17.6 ± 0.5	0.34 ± 0.004	0.09 ± 0.04	1.5e-13	405.9
21	1.0	(8.1,−13.2)	18.4 ± 0.5	0.33 ± 0.03	0.05 ± 0.03	1.5e-13	788.4
			NGC 7177				
1	1.4	(−17.1,2.1)	15.5 ± 0.5	0.46 ± 0.009	0.8 ± 0.01	5.1e-14	25.8
2	0.7	(−4.5,4.8)	17.6 ± 0.9	0.44 ± 0.03	0.69 ± 0.008	7.9e-15	27.4
3	1.0	(−3.0,6.0)	16.7 ± 0.6	0.45 ± 0.01	0.7 ± 0.008	1.5e-14	23.6
4	1.7	(−0.3,3.6)	15.0 ± 0.4	0.44 ± 0.002	0.78 ± 0.006	6.7e-14	22.8
5	1.7	(0.0,0.0)	15.0 ± 0.4	0.50 ± 0.02	0.88 ± 0.009	7.3e-14	21.2
6	1.4	(−6.0,−2.7)	17.0 ± 0.5	0.43 ± 0.006	0.71 ± 0.006	1.8e-14	34.4
7	1.7	(−2.7,−7.2)	16.5 ± 0.4	0.37 ± 0.006	0.71 ± 0.004	3.6e-14	46.7
8	1.4	(0.0,−8.7)	16.8 ± 0.5	0.35 ± 0.01	0.67 ± 0.008	2.0e-14	33.1
9	1.7	(5.7,−11.1)	15.3 ± 0.1	0.35 ± 0.005	0.56 ± 0.009	2.1e-14	9.3
10	1.7	(−13.8,−9.6)	17.7 ± 0.4	0.29 ± 0.006	0.56 ± 0.02	3.5e-14	139.4
11	1.4	(16.5,8.1)	18.2 ± 0.5	0.47 ± 0.04	0.85 ± 0.01	1.4e-14	79.7
			NGC 7469				
1	0.7	(2.1,3.9)	16.9 ± 0.9	0.42 ± 0.03	0.62 ± 0.002	1.3e-14	53.0
2	0.7	(0.0,4.2)	17.0 ± 0.9	0.39 ± 0.03	0.66 ± 0.02	1.3e-14	63.3
3	0.7	(−1.5,3.9)	17.1 ± 1.0	0.42 ± 0.01	0.62 ± 0.02	5.8e-15	58.2
4	0.7	(−2.7,3.6)	18.9 ± 0.9	0.61 ± 0.05	0.65 ± 0.02	8.4e-15	50.1
5	0.7	(−6.3,1.8)	19.1 ± 0.9	0.43 ± 0.01	0.58 ± 0.02	5.0e-15	39.1
6	0.3	(−8.7,−4.5)	19.9 ± 2.0	0.31 ± 0.03	0.48 ± 0.05	2.0e-15	37.9

Table 4 – *continued*

region number	radius ($''$)	distance from centre ($''$)	V	$V-R$ (mag)	$R-I$	$F(\mathrm{H}\alpha)$ (erg s^{-1} cm^{-2})	EW(Hα) (Å)
7	0.3	(−3.6,−8.1)	20.6 ± 2.0	0.41 ± 0.09	0.6 ± 0.1	1.5e-15	51.1
8	0.7	(0.0,−7.5)	19.1 ± 0.9	0.34 ± 0.02	0.5 ± 0.02	5.5e-15	47.6
9	0.7	(4.2,−1.5)	18.5 ± 0.9	0.50 ± 0.02	0.59 ± 0.02	8.4e-15	37.8
10	0.5	(4.2,0.3)	17.5 ± 0.7	0.54 ± 0.03	0.60 ± 0.01	2.6e-14	47.2
11	0.7	(3.9,2.7)	18.6 ± 1.0	0.59 ± 0.05	0.71 ± 0.003	8.8e-15	36.8

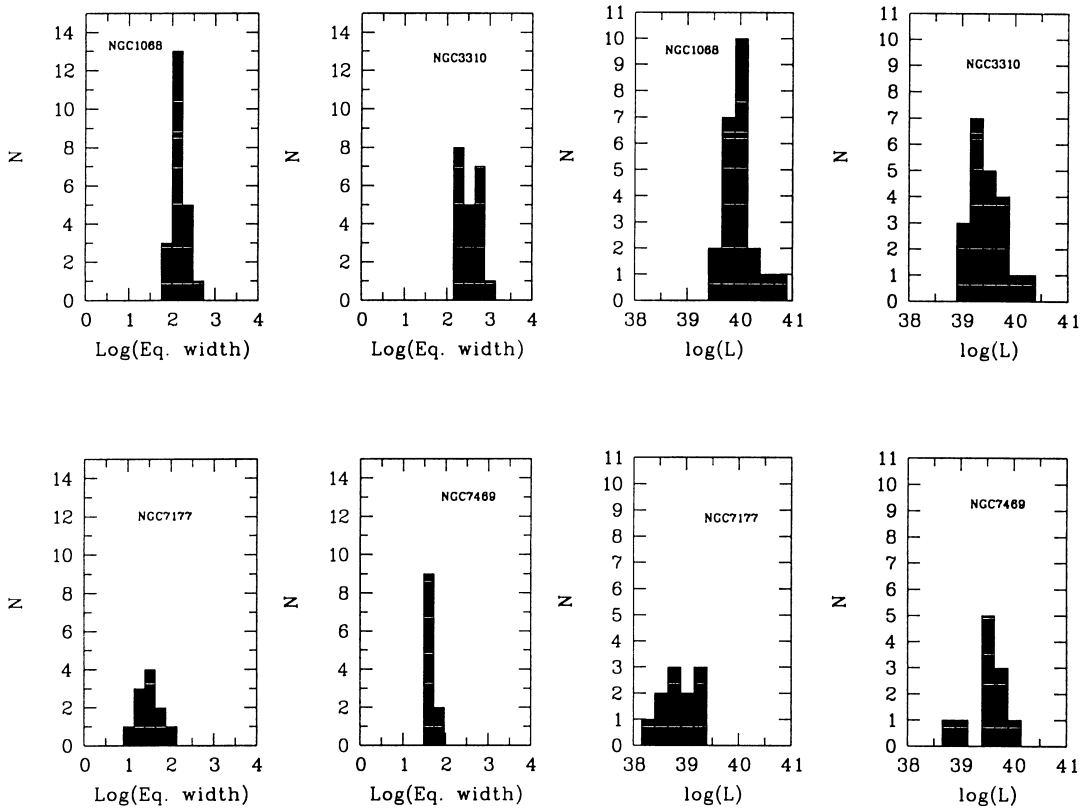

Figure 4. Histograms of luminosity and equivalent width of Hα for NGC 1068, 3310 and 7469, the peak in Hα luminosity is found at $\log L(\mathrm{H}\alpha) = 39.5$, while for NGC 7177 the luminosities seem to be, on average, lower by an order of magnitude. The medium value of log(EW) is around 2.5 for NGC 1068 and 3310, 1.9 for NGC 7469 and 1.5 for NGC 7177.

$\log L(\mathrm{H}\alpha) > 39.0$, which places them into the category of supergiant H II regions as defined by Kennicutt (1983). As can be seen in Fig. 4, for three of the galaxies: NGC 1068, 3310 and 7469, the peak Hα luminosity is found at $\log L(\mathrm{H}\alpha) = 39.5$, while for NGC 7177 the luminosities seem to be, in average, lower by an order of magnitude. The cumulative luminosity functions for the CNSFRs in each of the galaxies have been fitted by laws of the form $N(L) \propto L^{1-\alpha}$. The values of α obtained from the fits are close to the value of 2 found by Kennicutt (1983), except in the case of NGC 7469 for which $\alpha = 2.5$. An even steeper slope is found by González Delgado et al. (1997) for the high-luminosity disc H II regions of this galaxy. However, given the small number of points entering the fits and the systematic errors inherent to the method, this fact might not be significant.

The Hα luminosity versus size relation can be seen in Fig. 5. For each of the galaxies the data can be fitted in the log–log plane by a regression line of slope between 2 and 2.5. However, better fits are obtained for the regions in NGC 1068 and 3310 [$a = 2.2$, $\log L_o(\mathrm{H}\alpha) = 35.6$] and NGC 7177 and 7469 [$a = 2.2$, $\log L_o(\mathrm{H}\alpha) = 34.5$] taken separately. This seems to indicate that, for a given Hα luminosity, the CNSFRs in NGC 7177 and 7469 are larger and more diffuse than in the other two galaxies in which the regions seem to be more compact.

Regarding the properties of the stellar continuum, some information can be obtained by looking at the I versus $R-I$ colour–magnitude diagram, since our R images are corrected for Hα + [N II] emission and the I frame is almost emission-line free. Fig. 6 shows that in this diagram the regions of NGC 3310 are well separated from the rest, showing lower continuum luminosity and bluer colours. This can be partially because of their low metallicity (about 1/10 solar; Pastoriza et al. 1993). The CNSFRs in the other three galaxies show $R - I$ colours between 0.46 and 0.88. Since these colours are in most cases redder than the average value for their galactic discs – 0.50, 0.62 and 0.65 for NGC 1068, 7469 and 7177 respectively – they cannnot be attributed to a substantial background contribution not taken into account. Actually, any further background subtraction would produce even redder colours.

Hα equivalent widths also provide information about the stellar continuum properties. By combining the four histograms at the

Table 5. Linear sizes, absolute magnitudes and Hα luminosities of the observed H II regions.

region number	radius (pc)	distance (pc)	$M(V)$ (mag)	$M(R)$ (mag)	$M(I)$ (mag)	$\log L(\mathrm{H}\alpha)$ (erg s^{-1} cm^{-2})
			NGC 1068			
1	149.3	1545.1	−14.8	−15.3	−15.9	39.9
2	149.3	2037.9	−14.1	−14.4	−15.0	39.7
3	149.3	1790.8	−14.7	−15.1	−15.8	39.8
4	149.3	1641.9	−14.9	−15.4	−16.0	39.9
5	342.4	1968.9	−16.3	−16.7	−17.2	40.8
6	–	–	–	–	–	–
7	131.7	951.0	−16.1	−16.5	−17.1	40.0
8	131.7	968.0	−15.7	−16.1	−16.7	40.1
9	131.7	1192.0	−16.1	−16.4	−17.0	40.1
10	193.2	1285.6	−16.3	−16.6	−17.3	40.4
11	140.5	1264.1	−15.5	−16.0	−16.6	40.1
12	≤79.1	1202.9	−14.9	−15.4	−16.0	39.6
13	175.4	1239.2	−15.2	−15.7	−16.3	40.1
14	114.1	943.7	−15.0	−16.3	−16.8	39.9
15	114.1	1085.4	−15.7	−16.0	−16.5	39.9
16	114.1	884.9	−15.5	−15.8	−16.4	39.8
17	114.1	1175.5	−14.9	−15.3	−15.8	39.8
18	114.1	1332.2	−14.5	−14.9	−15.4	39.9
19	210.7	1368.1	−16.2	−16.8	−17.3	40.4
20	175.6	1379.5	−16.6	−17.0	−17.6	40.3
21	140.5	1296.3	−15.1	−15.6	−16.1	40.0
22	–	–	–	–	–	–
23	114.1	774.2	−15.0	−15.4	−16.0	39.9
A	114.1	1790.5	−14.3	−14.8	−15.2	39.6
B	140.5	1854.7	−14.7	−15.1	−15.6	39.8
			NGC 3310			
1	41.2	657.0	−11.2	−11.5	−11.7	39.1
2	61.8	635.0	−12.9	−13.3	−13.4	39.5
3	81.8	374.8	−14.2	−14.4	−14.6	40.0
4	61.8	343.0	−14.0	−14.2	−14.4	39.8
5	41.2	351.1	−13.3	−13.5	−13.8	39.5
6	61.8	382.2	−13.6	−13.9	−14.1	39.4
7	61.8	431.0	−13.6	−13.8	−14.0	39.3
8	41.2	203.3	−13.0	−13.3	−13.6	39.0
9	61.8	272.7	−13.6	−13.9	−14.1	39.2
10	61.8	309.1	−13.6	−13.9	−14.2	39.2
11	61.8	406.5	−13.7	−14.0	−14.3	39.3
12	81.8	512.0	−14.5	−14.8	−14.9	39.7
13	61.8	625.6	−13.9	−14.1	−14.3	39.4
14	61.8	339.6	−13.7	−14.1	−14.3	39.5
15	41.2	570.9	−12.0	−12.4	−12.6	39.2
16	61.8	436.7	−13.4	−13.8	−13.9	39.8
17	41.2	620.5	−12.0	−12.3	−12.5	38.9
18	61.8	595.5	−13.6	−13.9	−13.9	39.7
19	103.0	682.4	−14.8	−15.0	−15.0	40.3
20	61.8	1480.5	−12.9	−13.3	−13.2	39.4
21	61.8	938.5	−12.1	−12.5	−12.5	39.4
			NGC 7177			
1	100.2	1277.9	−15.4	−15.9	−16.7	39.2
2	≤50.5	488.0	−13.3	−13.8	−14.4	38.3
3	75.7	497.6	−14.2	−14.7	−15.4	38.6
4	126.1	268.0	−15.9	−16.4	−17.2	39.3
5	126.1	0	−15.9	−16.4	−17.3	39.3
6	100.2	488.0	−13.9	−14.4	−15.1	38.7
7	126.1	570.4	−14.4	−14.8	−15.5	39.0
8	100.2	645.3	−14.1	−14.5	−15.2	38.8
9	126.1	925.6	−15.6	−16.0	−16.5	38.8
10	126.1	1246.9	−13.2	−13.5	−14.0	39.0
11	100.2	1363.4	−12.7	−13.2	−14.0	38.6
			NGC 7469			
1	214.3	1395.8	−17.1	−17.5	−18.2	39.8
2	214.3	1323.5	−17.1	−17.5	−18.1	39.8
3	214.3	1316.7	−17.0	−17.4	−18.0	39.5
4	214.3	1418.0	−15.2	−15.8	−16.4	39.6
5	214.3	2064.7	−15.0	−15.4	−16.0	39.4

Table 5 – *continued*

region number	radius (pc)	distance (pc)	$M(V)$ (mag)	$M(R)$ (mag)	$M(I)$ (mag)	$\log L(\mathrm{H}\alpha)$ ($\mathrm{erg\,s^{-1}\,cm^{-2}}$)
6	≤107.1	3086.6	−14.1	−14.4	−14.9	39.0
7	≤107.1	2793.2	−13.5	−13.9	−14.5	38.9
8	214.3	2363.4	−14.9	−15.3	−15.8	39.4
9	214.3	1405.4	−15.5	−16.0	−16.6	39.6
10	214.3	1326.9	−16.5	−17.1	−17.7	40.1
11	160.7	1494.8	−15.5	−16.1	−16.8	39.7

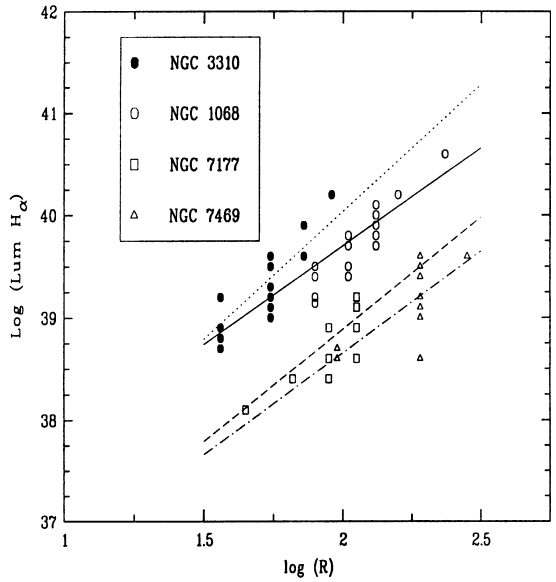

Figure 5. Logarithmic relation between Hα luminosity radius for each individual H II region. The different lines represent functions $\log L = a \log R + b$ where a is nearly 2 in all cases.

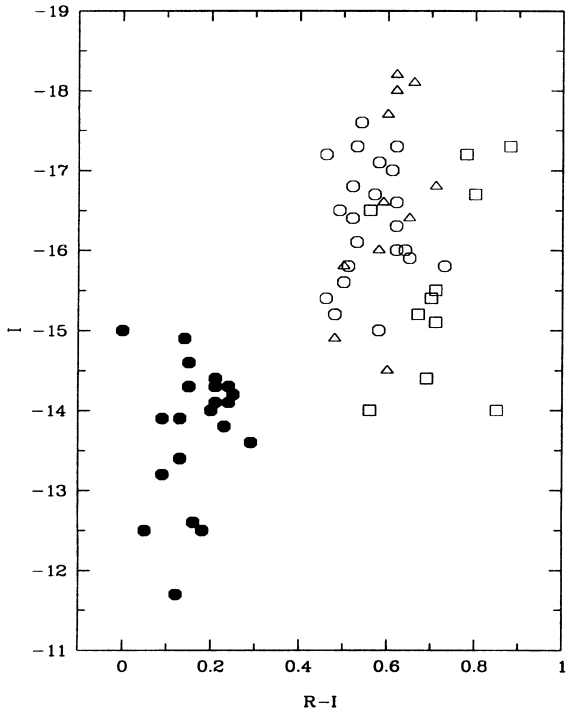

Figure 6. M_I versus $R - I$ colour-magnitude diagram for all the H II regions of the sample. Symbols as in Fig. 5.

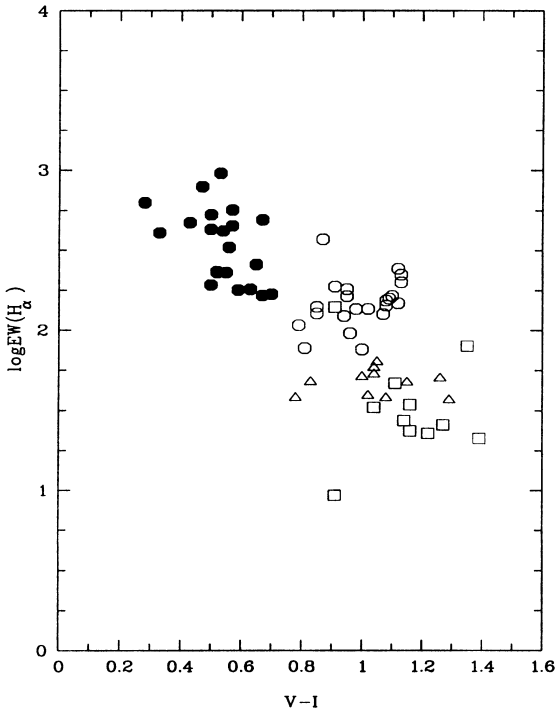

Figure 7. M_I versus equivalent width of Hα versus $V - I$ colour for all the H II regions of the sample. Symbols as in Fig. 5.

left of Fig. 4, it can be seen that the distribution of EW(Hα) is double peaked. While NGC 1068 and NGC 3310 show values centred about $\log \mathrm{EW}(\mathrm{H}\alpha) = 2.4$, those corresponding to NGC 7177 and 7469 are clustered around $\log \mathrm{EW}(\mathrm{H}\alpha) = 1.5$ implying that either their regions are more evolved or the contribution by a non-ionizing population is more important for the regions in these last two galaxies.

In fact, when plotting $\log \mathrm{EW}(\mathrm{H}\alpha)$ versus $V - I$ colour (Fig. 7) a relation seems to emerge with regions with larger equivalent widths showing bluer colours. Since the equivalent width of Hα is a good age indicator for ionized regions, we are tempted to attribute this relation to age rather than metallicity.

3.3 Comparison with earlier photometry

There is not much broad-band photometry of H II regions. Our results can be compared with those of Mayya (1994) and Telles & Terlevich (1997). The objects studied by Mayya are mainly disc H II regions for which V, R and Hα photometry is given. On the other hand, Telles & Terlevich provide V, R, I and Hα photometry for H II galaxies.

Fig. 8 shows the absolute V magnitude (left panel) and the logarithm of the equivalent width of Hα (right panel) versus $V - R$

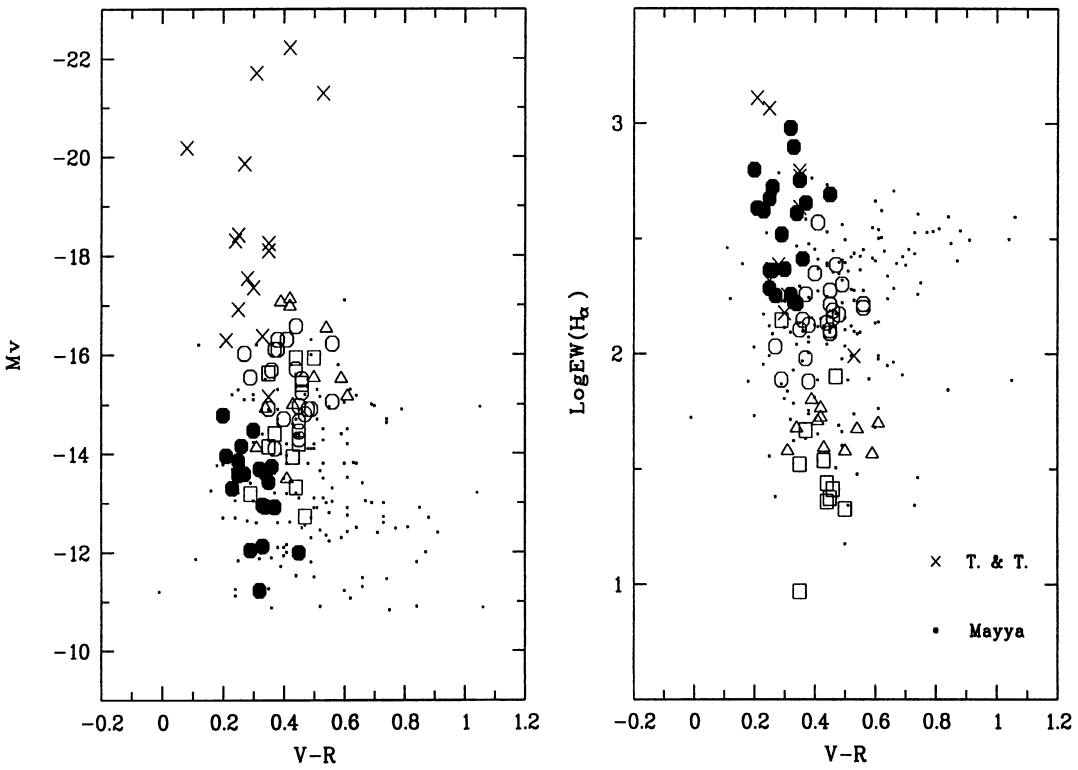

Figure 8. Colour–magnitude and colour versus log EW(Hα) for our data and those found in the literature. Symbols as in Fig. 5 with added × from Telles & Terlevich (1997) and dots from Mayya (1994).

colour for our objects together with those of Mayya and Telles & Terlevich. H II galaxies are the brightest objects in the plot, while some disc H II regions are at the lower luminosity end. CNSFRs show an intermediate behaviour. Except for some low-luminosity disc H II regions which look redder, all the objects show similar $V-R$ colours. These regions also have rather large Hα equivalent widths and so their excess R flux might be due to the contribution of the Hα emission.

Regarding equivalent widths, the regions of NGC 3310 have values comparable to those found in H II galaxies while the CNSFRs in the rest of the galaxies have EW(Hα) similar to those found in disc H II regions.

4 DISCUSSION

4.1 Evolutionary synthesis models

Our results can be interpreted with the help of evolutionary population synthesis models. Leitherer & Heckman (1995) provide broad-band colours and Hα luminosities and equivalent widths for different populations that can be directly compared with our data. Models for both instantaneous bursts and continuous star formation computed with different initial mass functions (IMFs) are given. The assumed metallicities range from 0.1 to 2 times solar. We have used for comparison the models with metallicity 0.25 solar for the regions of NGC 3310 in agreement with oxygen abundance determinations for some of their CNSFRs (Pastoriza et al. 1993). Solar metallicity models have been adopted for the rest of the galaxies. In all cases a Salpeter IMF has been assumed.

Fig. 9 (top left panel) shows the run of instantaneous burst subsolar (solid line) and solar (dashed line) models in the $V-R$ versus $R-I$ colour–colour diagram as compared with data. Each tick on the lines corresponds to 1 Myr from 1 to 10 Myr and 5 Myr for 10 to 40 Myr The end of the line corresponds to an age of about 300 Myr. It can be seen that, as the cluster evolves from 1 to 3 Myr, its $V-R$ colour decreases at a constant $R-I$ value, as the V flux increases. From then onwards the general trend is for the colours to get redder with time. The reddest colours reached by the subsolar model are about $V-R=0.25$ and $R-I=0.5$. For the solar metallicity models the evolutionary track moves vertically upwards for ages between 6 and 7 Myr and downwards for ages between 10 and 15 Myr.

The effect of 1 magnitude extinction would move the model points up and to the right by the amount indicated by the arrow in the plot. This diagram is also affected by the emission of [O III] in the V filter. This line is significant only at low metallicities and very young ages (Stasińska & Leitherer 1996) but its maximum effect would be to move downwards the points by about 0.005 mag in $V-R$. This uncertainty is in most cases smaller than the average observational error also shown in the plot.

In the absence of reddening, the colours of the regions of NGC 3310 can be reproduced by single burst populations of age between 7 and 10 Myr. Different amounts of extinction, between 0.5 and 1.5 mag, would allow younger ages. The extinction derived for some of these regions from spectroscopic data are between 0.4 and 1.15 mag (Pastoriza et al. 1993).

For the rest of the regions, the observed colours can be adequately reproduced by single burst populations with age between 7 to 300 Myr, the maximum age computed by Leitherer & Heckman, if different amounts of extinction are assumed. Continuous star formation models provide, in general, a poorer fit to the data. Higher ages (30 to 100 Myr) are found

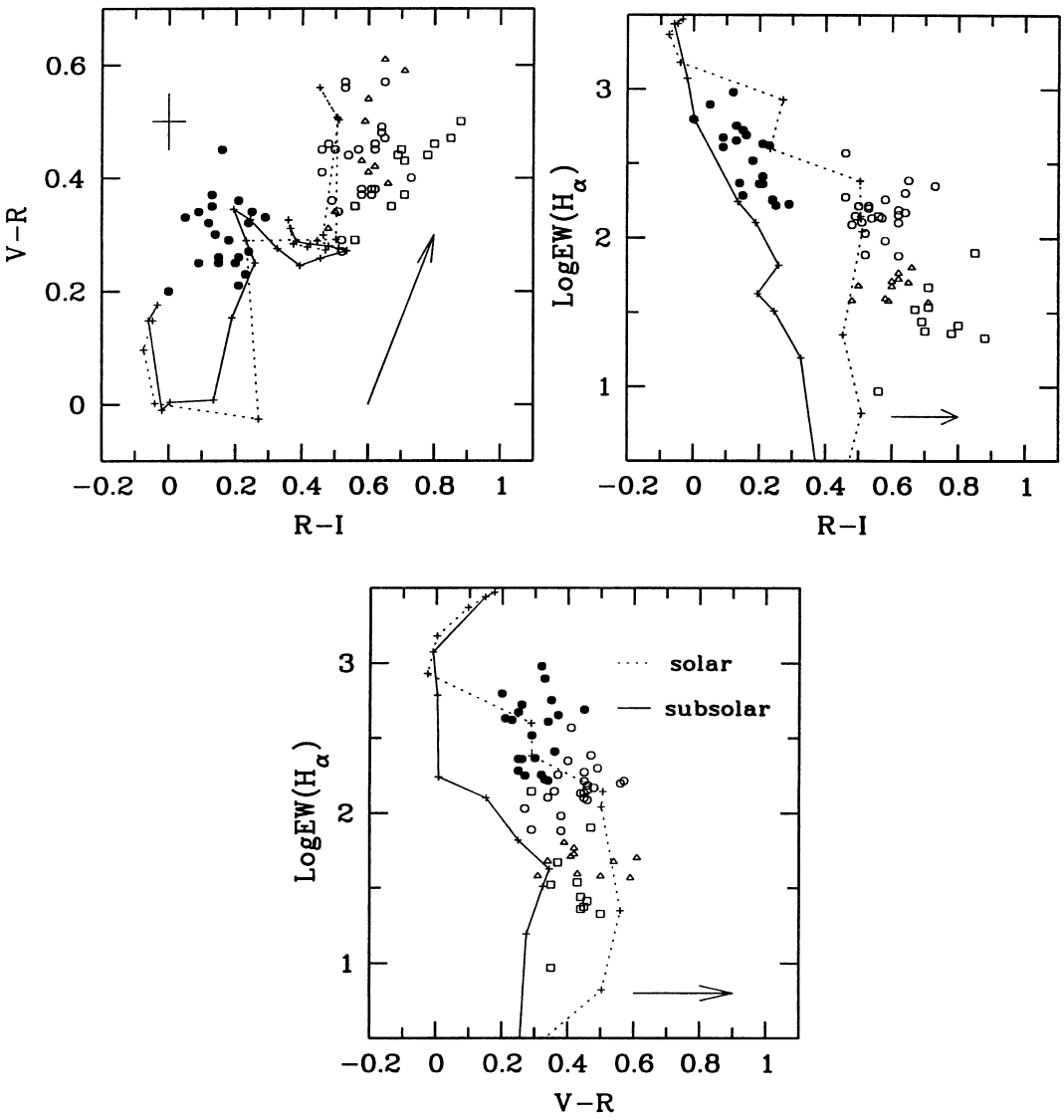

Figure 9. $V-R$ versus $R-I$ and equivalent width of Hα versus $R-I$ and versus $V-R$ diagrams for a single burst stellar population for solar and subsolar metallicities. The effect of reddening ($A_v = 1$ mag) is plotted in the bottom right of the figures, as well as a typical error bar in the top-left one. Symbols as in Fig. 5.

using this kind of model and visual extinctions larger than 2 mag are, in many cases, necessary to reproduce the observed colours.

Further insight can be gained by looking at the behaviour of equivalent width of Hα versus $R-I$ colour predicted by the models (Fig. 9, top-right panel), since it provides information about the ionizing stars. The large equivalent widths observed in the regions of NGC 3310 can only be reproduced by very young populations with ages between 3 and 5 Myr. Values of extinction less than 0.7 mag are therefore implied. The ionizing population of the regions in NGC 1068, 7469 and 7177 seems to be progressively older, being in most cases between 6 and 9 Myr. The models with contiuous star formation that best reproduce the observed colours cannot reproduce the moderate values of the equivalent widths of Hα which are observed and therefore have not been pursued further.

On the other hand, as already mentioned in the previous section, a relation seems to exist between log EW(Hα) and $R-I$. If interpreted as an extinction effect, this would imply an increasing extinction from NGC 1068 to 7177. However, no relation is apparent between log EW(Hα) and $V-R$ (Fig. 8) where the effects of extinction should be more important. The difference in $R-I$ can also be attributed to an increasing contribution of red supergiant stars (García-Vargas, Mollá & Bressan 1998) which could be associated with an underlying non-ionizing population.

4.2 The case for a two-burst population model

The two graphs just discussed generate a three dimensional space in which two dimensions (the $R-I$ and $V-R$ colours) represent basically the stellar continuum properties, while the third one (equivalent width of Hα) stands for the importance of the gas emission relative to the stellar continuum. For a model with given metallicity and initial mass function, a zero-age single burst population is represented in this space by a point. As time goes on, this point should move along the track given by the theoretical model. Several effects could move data away from this theoretical

line: the presence of reddening, the contribution of emission lines to the continuum band filters and the contribution of an extra non-ionizing stellar continuum flux. The second of these effects is actually negligible, except for very low metallicities and very low ages.

Taking this into account, consistent solutions for single burst populations can be found only for some of the regions of NGC 1068. In this case the burst ages are between 6 and 7 Myr and the derived visual extinctions are always less than 1 mag. For the rest of the regions, no consistent solutions for single burst populations are found, since different amounts of extinction are needed to reconcile models and data in each of the diagrams.

Therefore we have computed simple two-population models by combining young ionizing populations, with ages between 1 and 10 Myr, and non-ionizing underlying populations, with ages between 8 and 20 Myr (for ages older that 20 Myr the $V-R$ and $R-I$ colours remain practically constant within our observational errors), taken in different proportions. For each population pair, we have calculated the value of the equivalent width of Hα with increasing contribution of the young component to the total mass. For each studied region, the intersection of the line of observed EW(Hα) with the model lines gives the possible solutions. The procedure is illustrated in Fig. 11. Once the possible models have been selected, we have calculated the corresponding $V-R$ and $R-I$ colours and have compared them with the observed ones. Then we have chosen the solution than minimizes the difference between observed and calculated colours. No reddening is assumed for any of the two populations.

The selected models for each region and their characteristics are listed in Table 6, and shown in Fig. 10. The best models for the regions in NGC 3310 correspond to the combination of a young population 2.5 Myr old and an older one 8 Myr old, taken in different proportions as indicated in the table. For NGC 1068 the best combination corresponds to bursts of 5 and 9 Myr and these ages are increased to 8 and 15 Myr for NGC 7177 and 7469. In most cases, the age difference between the two components may be consistent with the time elapsed in the models for the first supernovae to explode. According to Leitherer & Heckman's models this time is around 3.6 Myr both for metallicities solar and 0.25 solar and the expected supernova rate is $10^{-3}\,\mathrm{yr}^{-1}$ during a period of about 25 Myr.

Columns 3 and 4 in Table 6 give the model computed colours while columns 5 and 6 give the difference between observed and computed colours. In most cases the computed $V-R$ colour agrees with the observed one within the errors, this is also true for the $R-I$ colour of the regions of NGC 3310. However, for the rest of the regions a considerable excess on the observed $R-I$ colour over the computed one is found, which is not consistent with a normal reddening law. ($R-I$) colours of red supergiant stars are between 0.4 and 1.00 (Díaz, Terlevich & Terlevich 1989), which is actually the range covered by our observed H II regions. Therefore, if this near infrared excess is attributed to the presence

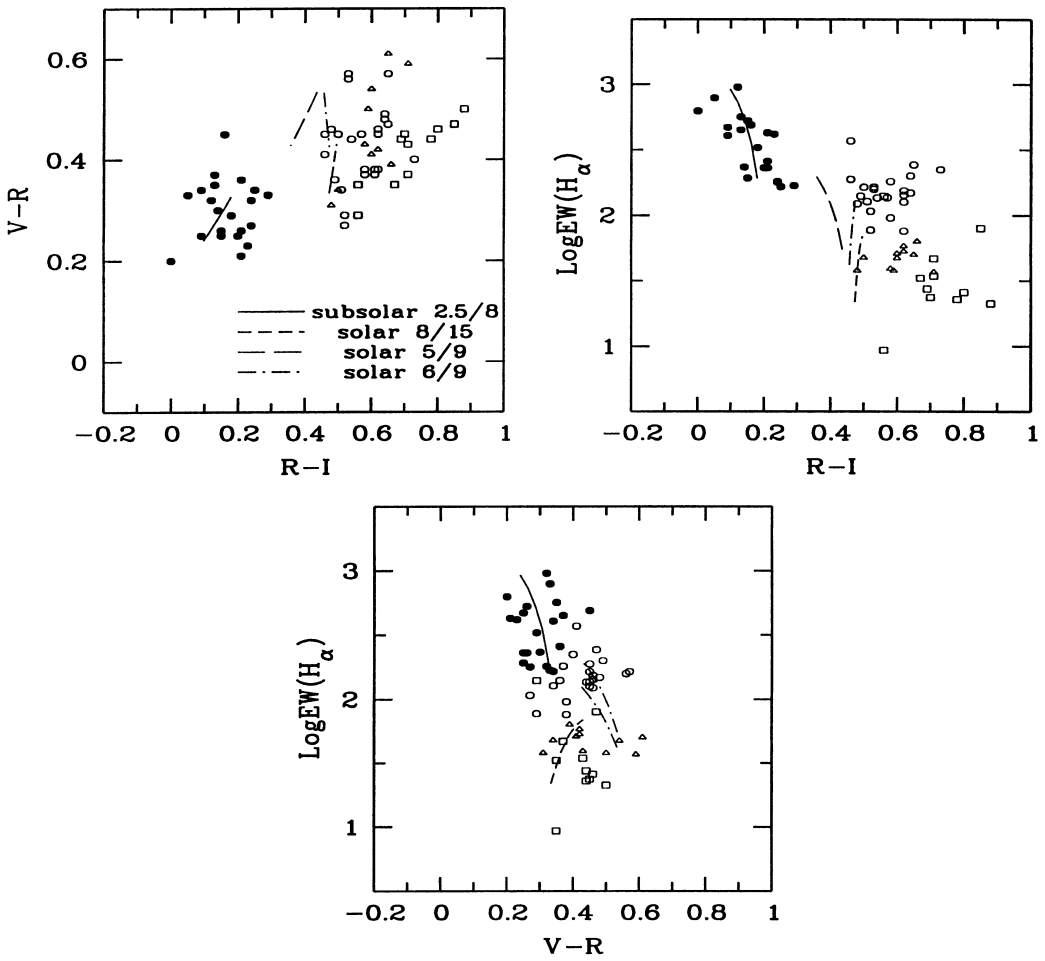

Figure 10. Same as Fig. 9 but for a two-burst stellar population.

Table 6. Mass contribution of the younger burst (M_y) to the total stellar mass of the H II region (M_t), computed colours and differences (CD) between the observed colours and those given by the models.

Region	M_y/M_t per cent	$(V-R)$	$(R-I)$	CD$(V-R)$	CD$(R-I)$
		NGC 1068	5/9 Myr		
1	61	0.40	0.33	0.07	0.32
2	46	0.44	0.37	−0.07	0.21
3	57	0.41	0.34	−0.01	0.38
4	51	0.43	0.36	0.06	0.28
5	92	0.31	0.26	0.1	0.20
6	–	–	–	–	–
7	22	0.50	0.41	−0.13	0.18
8	33	0.47	0.39	−0.03	0.19
9	33	0.47	0.39	−0.09	0.21
10	16	0.52	0.43	−0.08	0.19
11	38	0.46	0.38	0.00	0.23
12	37	0.46	0.39	0.02	0.25
13	35	0.47	0.39	−0.01	0.23
14	25	0.49	0.41	−0.22	0.11
15	35	0.47	0.39	−0.11	0.10
16	17	0.52	0.42	−0.23	0.10
17	31	0.48	0.40	−0.13	0.12
18	48	0.43	0.36	0.02	0.10
19	41	0.45	0.38	0.11	0.15
20	33	0.47	0.39	−0.03	0.15
21	40	0.46	0.38	0.10	0.15
22	–	–	–	–	–
23	31	0.48	0.40	−0.03	0.22
A	30	0.48	0.40	−0.03	0.09
B	41	0.45	0.38	0.00	0.12
		NGC 3310	2.5/8 Myr		
1	52	0.24	0.09	0.08	0.03
2	26	0.29	0.15	0.08	−0.02
3	30	0.29	0.14	−0.03	0.01
4	24	0.30	0.15	−0.09	0.06
5	24	0.30	0.15	−0.07	0.08
6	13	0.32	0.17	−0.06	0.04
7	13	0.32	0.17	−0.07	0.03
8	9	0.33	0.18	0.00	0.11
9	9	0.33	0.18	−0.06	0.06
10	8	0.33	0.18	0.01	0.07
11	9	0.33	0.18	−0.01	0.06
12	13	0.32	0.17	−0.02	−0.03
13	10	0.33	0.18	−0.08	−0.03
14	14	0.33	0.17	0.03	0.04
15	28	0.29	0.15	0.16	0.01
16	32	0.28	0.14	0.07	−0.01
17	19	0.31	0.16	−0.02	0.02
18	27	0.29	0.15	−0.04	−0.06
19	35	0.27	0.13	−0.07	−0.13
20	23	0.30	0.16	0.04	−0.07
21	44	0.26	0.11	0.07	−0.06
		NGC 7177	8/15 Myr		
1	12	0.34	0.48	0.12	0.32
2	13	0.34	0.48	0.10	0.21
3	11	0.34	0.47	0.11	0.23
4	11	0.34	0.47	0.10	0.31
5	9	0.33	0.47	0.17	0.41
6	18	0.36	0.48	0.07	0.23
7	26	0.38	0.48	−0.01	0.23
8	17	0.35	0.48	0.00	0.19
9	3	0.31	0.47	0.04	0.09
10	56	0.41	0.48	−0.12	0.08
11	57	0.44	0.50	0.03	0.35
		NGC 7469	8/15 Myr		
1	32	0.39	0.49	0.03	0.13
2	40	0.41	0.49	−0.02	0.17
3	36	0.40	0.49	0.02	0.13
4	29	0.39	0.49	0.22	0.16
5	21	0.37	0.48	0.06	0.1

Table 6 – *continued*

Region	M_y/M_t per cent	$(V-R)$	$(R-I)$	CD$(V-R)$	CD$(R-I)$
6	20	0.36	0.48	−0.05	0.00
7	30	0.39	0.49	0.02	0.11
8	27	0.38	0.48	−0.04	0.02
9	20	0.36	0.48	0.14	0.11
10	27	0.38	0.48	0.26	0.12
11	19	0.36	0.48	0.23	0.23

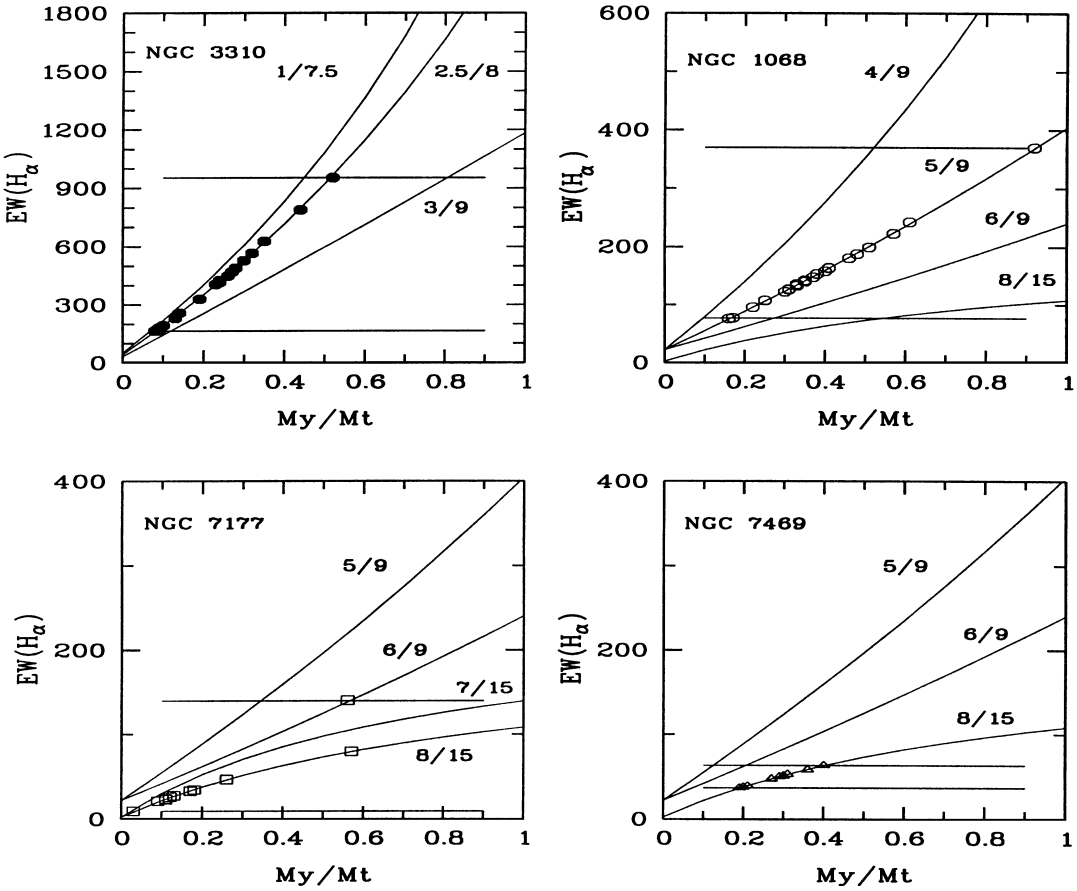

Figure 11. Two-burst models that reproduce the equivalent width of Hα, as a function of the fraction of the young burst mass. Horizontal lines correspond to the maximum and minimum values of EW(Hα) measured in each galaxy CNSFRs. Several options are displayed and the regions are overplotted over the chosen best couple of ages.

of a red supergiant population, this seems to imply that this population is not properly taken into account by the models.

Two-burst populations have also been found for the circumnuclear regions of NGC 3310 studied spectroscopically by Pastoriza et al. (1993); also Mayya & Prabhu (1996), from a study of disc H II regions, find in most cases evindence for an accompanying population rich in red supergiants from a previous burst and Kennicutt, Keel & Blaha (1989) mention the possibility that star formation in 'hot spots' takes place over time-scales much longer than in normal disc H II regions in order to explain the lower values of Hα equivalent widths found for the former objects.

If this two-population scenario is adopted, there is some indication for the CNSFR in NGC 7177 and 7469, LINER and Seyfert type 1 respectivey, to be older than those of NGC 1068, Seyfert type 2, which in turn look older than those of NGC 3310, a starburst galaxy. More observations are obviously needed in order to test if the history of the circumnuclear star formation activity is related to the nuclear type of the parent galaxy.

5 SUMMARY AND CONCLUSIONS

We have studied 68 star-forming complexes around four galactic nuclei showing different degrees of activity. For all of them we have obtained Hα fluxes, luminosities and equivalent widths, sizes, *V*, *R* and *I* magnitudes and $V-R$ and $R-I$ colours.

The linear diameters of the regions range from 82.4 to 684.8 pc and their Hα luminosities range from 2×10^{38} to 7×10^{40} erg, which places them in the category of supergiant H II regions according to the classification given by Kennicutt (1983).

The regions of NGC 7177 are about an order of magnitude less luminous than the others and it seems that, for a given Hα luminosity, the regions in NGC 7177 and NGC 7469 are larger and

more diffuse than in the other two galaxies in which the regions seem to be more compact. The distribution of $\log \mathrm{EW}(\mathrm{H}\alpha)$ in the observed CNSFRs is double-peaked: the regions in NGC 1068 and 3310 show values centred at about 2.4 while those of NGC 7177 and 7469 are clustered around 1.5 implying that either these last regions are more evolved or the contribution by a non-ionizing population is more important.

Regarding the colours it seems that the regions in NGC 3310 show bluer continuum colours than the rest. This is probably owing to a mixed effect of a younger age and a lower metallicity.

If we compare the observed colours ($V - R$ and $R - I$) and Hα equivalent widths with those predicted by theoretical evolutionary synthesis models we find that, except for a few regions in NGC 1068, in most of the observed regions the data cannot be adequately reproduced by a combination of a single burst of star formation and a normal reddening law. The best fitting models involve a composite population with two clusters of ages 5 and 9 Myr in the case of NGC 1068, 2.5 and 8 Myr for NGC 3310, and 8 and 15 Myr in the cases of NGC 7177 and 7469. The contribution to the total cluster mass by the younger component is found to be between 3 and 61 per cent. The age difference between the two assumed bursts is consistent with the time elapsed in the models until the supernovae explosions from the first burst take place.

Under this two-population scenario the CNSFR of NGC 7469 and 7177 (Seyfert 1 and LINER respectively) are found to be older than the corresponding ones in NGC 1068 (Seyfert 2) and NGC 3310 (starburst). More observations are needed to establish if the age of the CNSFR and the nuclear type of the galaxy are related to one another.

ACKNOWLEDGMENTS

The JKT is operated in the island of La Palma by the Issac Newton Group in the Spanish Observatorio del Roque de los Muchachos of the Instituto de Astrofísica de Canarias. We would like to thank CAT for awarding observing time. We also would like to thank VILSPA and LAEFF for kind support with the first reduction of our data. We also thank an anonymous referee for her/his comments and suggestions.

ET is grateful to an IBERDROLA Visiting Professorship to UAM during which this work was completed. This work has been partially supported by DGICYT project PB-96-052.

REFERENCES

Antonucci R. R. J., Miller J. S., 1985, ApJ, 297, 476
Arsenault R., 1989, A&A, 217, 66
Athanassoula E., 1992, MNRAS, 259, 345
Barth A. J. et al., 1995, AJ, 110, 1009
Bessell M. S., 1990, PASP, 102, 1181
Bottinelli L., Gouguenheim L., Paturel G., De Vaucouleurs G., 1984, A&AS, 56, 381
Burstein D., Heiles C., 1984, ApJS, 54, 33
Buta R., Crocker D. A., 1993, AJ, 105, 1344
Combes F., Gerin M., 1985, A&A, 150, 327
De Vaucouleurs G., De Vaucouleurs A., Corwin H. G., Buta R. J., Paturel G., Fouqué P., 1991, Third Reference Catalog of Bright Galaxies, Springer, Berlin, (RC3)
Díaz A. I., Terlevich E., Terlevich R., 1989, MNRAS, 239, 325
Elmegreen G. B., 1994, ApJ, 425, L73
Elmegreen G. B., 1997, Rev. Mex. Astron. Astrofis. (Serie de Conferencias), 6, 165
García-Vargas M. L., González-Delgado R. M., Pérez E., Alloin D., Díaz A. I., Terlevich E., 1997, ApJ, 478, 112
García-Vargas M. L., Mollá M., Bressan A., 1998, A&AS, 130, 513
González Delgado R. M., Pérez E., Tadhunter C., Ví space=.2>lchez J. M., Rodriguez-Espinosa J. M., 1997, ApJS, 108, 199
González-Delgado R. M., Pérez E., Díaz A. I., García-Vargas M. L., Terlevich E., Vílchez J. M., 1995, ApJ, 439, 604
Hodge P. W., 1982, AJ, 87, 1341
Holtzman J. A. et al., 1992, AJ, 103, 691
Kennicutt R., 1983, ApJ, 272, 54
Kennicutt R., Keel W. C., Blaha C. A., 1989, AJ, 97, 1022
Landolt A. U., 1983, AJ, 88, 439
Leitherer C., Heckmann T., 1995, ApJS, 96, 9
Massey P., Strobel K., Barnes J. V., Anderson E., 1988, ApJ, 328, 315
Mauder W., Weigett G., Appenzeller I., Wagner S. J., 1994, A&A, 285, 44
Mayya Y. D., 1994, AJ, 108, 1276
Mayya Y. D., Prabhu T. P., 1996, AJ, 111, 1254
Norman S. T., Scoville N. Z., 1987, ApJ, 312, L39
Pastoriza M. G., Dottori H. A., Terlevich E., Terlevich R., Díaz A. I., 1993, MNRAS, 260, 177
Planesas P., Scoville N., Myers S. T., 1991, ApJ, 369, 364
Pogge R. W., 1989, ApJS, 71, 433
Sánchez Portal M., Díaz A. I., Terlevich R., Terlevich E., Álvarez Álvarez M., Aretxaga I., 1999, MNRAS, in press
Sandage A., Tammann G. A., 1975, ApJ, 196, 313
Scoville N. Z., Matthews K., Carico D. P., Sanders D. B., 1988, ApJ, 327, L61
Seaton M. J., 1979, MNRAS, 187, 73P
Sérsic J. L., Pastoriza M. G., 1967, PASP, 79, 152
Smith D. A. et al., 1996, ApJ, 473, L21
Stasińska G., Leitherer C., 1996, ApJS, 107, 661
Stone R. P. S., 1977, ApJ, 218, 767
Telesco C. M., Dressel L. L., Wolstencroft R. D., 1993, ApJ, 414, 120
Telles E., Terlevich R., 1997, MNRAS, 286, 183
Terlevich E., Díaz A. I., Terlevich R., 1990a, MNRAS, 242, 271
Terlevich E., Díaz A. I., Pastoriza M. G., Terlevich R., Dottori H., 1990b, MNRAS, 242, 48P
Terlevich R., Sánchez Portal M., Díaz A. I., Terlevich E., 1991, MNRAS, 249, 36
Verter F., 1985, ApJS, 57, 261
Weedman D. W., 1983, ApJ, 226, 479
Wilson A. S., Baldwin J. A., Sun S.-D., Wright A. E., 1986, ApJ, 310, 121
Wilson A. S., 1991, ApJ, 381, 79

This paper has been typeset from a TEX/LATEX file prepared by the author.